

TDGCN-Based Mobile Multiuser Physical-Layer Authentication for EI-Enabled IIoT

Rui Meng, Hangyu Zhao, Bingxuan Xu, Yining Wang, Xiaodong Xu, *Senior Member, IEEE*,
Suyu Lv, Xiaofeng Tao, *Senior Member, IEEE*, and Ping Zhang, *Fellow, IEEE*

Abstract—Physical-Layer Authentication (PLA) offers endogenous security, lightweight implementation, and high reliability, making it a promising complement to upper-layer security methods in Edge Intelligence (EI)-empowered Industrial Internet of Things (IIoT). However, state-of-the-art Channel State Information (CSI)-based PLA schemes face challenges in recognizing mobile multi-users due to the limited reliability of CSI fingerprints in low Signal-to-Noise Ratio (SNR) environments and the constantly shifting CSI distributions with user movements. To address these issues, we propose a Temporal Dynamic Graph Convolutional Network (TDGCN)-based PLA scheme. This scheme harnesses Intelligent Reflecting Surfaces (IRSs) to refine CSI fingerprint precision and employs Graph Neural Networks (GNNs) to capture the spatio-temporal dynamics induced by user movements and IRS deployments. Specifically, we partition hierarchical CSI fingerprints into multivariate time series and utilize dynamic GNNs to capture their associations. Additionally, Temporal Convolutional Networks (TCNs) handle temporal dependencies within each CSI fingerprint dimension. Dynamic Graph Isomorphism Networks (GINs) and cascade node clustering pooling further enable efficient information aggregation and reduced computational complexity. Simulations demonstrate the proposed scheme's superior authentication accuracy compared to seven baseline schemes.

Index Terms—Physical-Layer Authentication (PLA), mobile multiuser authentication, IIoT, Deep Learning (DL).

I. INTRODUCTION

BY connecting sensors, devices, machines, and other industrial facilities through the Internet and communication technologies, Industrial Internet of Things (IIoT) can enable data collection, analysis, and sharing, ultimately optimizing production processes, monitoring device status, as well as predicting maintenance needs, in various industrial sectors like manufacturing, energy, transportation, and agriculture [1]. Compared with the mobile cloud computing-based IIoT with

long propagation delay and limited channel capacity, Edge Intelligence (EI)-enabled IIoT integrates Artificial Intelligence (AI) into edge networks to reduce latency and bandwidth requirements, improve real-time decision-making capability, and enhance data privacy and security [2].

Despite the continuous efforts to enhance security of EI-enabled IIoT, challenges remain in ensuring the security of identities and protecting data privacy [3]. Edge devices often necessitate communication with diversity devices and systems, such as cloud servers and end nodes. Unfortunately, the inherent openness of radio channels makes these communications susceptible to potential eavesdropping, interception, and forgery attacks. Furthermore, as edge devices are situated at the periphery of IIoT, they become more vulnerable to security threats [4]. To mitigate such security risks, identity identification plays a crucial role in verifying the legitimacy of users, devices or entities, thereby guaranteeing that only authorized devices can access protected resources and information [5].

Conventional authentication approaches rely on the widely adopted Public Key Infrastructure (PKI) framework, which leverages public key cryptography to facilitate secure communication. PKI encompasses a comprehensive range of technologies, policies, and procedures that govern the creation, distribution, and revocation of digital certificates [5]. However, the computational overhead associated with such methods can be burdensome for industrial devices [6]. Additionally, key management processes will introduce significant transmission latency, which fails to meet the demands of low-latency applications, such as real-time monitoring [7].

Physical-Layer Authentication (PLA) presents a promising supplementary approach to traditional upper-layer authentication methods [8]. By leveraging the distinct random characteristics of communication links and equipment-related features, PLA can provide inherently secure identity protection for transmitters [9]. This becomes particularly advantageous in EI-empowered IIoT, because edge servers are physically proximate to end devices and can conveniently acquire physical-layer attributes [7], such as Received Signal Strength (RSS) [6], Channel State Information (CSI) [7], [9], and radio frequency (RF) fingerprints [10]. Among these attributes, CSI reflects fine-grained channel characteristics and can be readily obtained without numerous upper-layer signaling processes or complex pre-processing techniques [8]. Therefore, the CSI-based PLA emerges as an ideal solution to ensure the identity security of IIoT end users [7].

In earlier literature, traditional PLA methods are commonly formulated as a statistical hypothesis test, in which the de-

(Corresponding author: Xiaodong Xu)

Rui Meng, Bingxuan Xu, and Yining Wang are with the State Key Laboratory of Networking and Switching Technology, Beijing University of Posts and Telecommunications, Beijing 100876, China (e-mail: buptmengrui@bupt.edu.cn; xubingxuan@bupt.edu.cn; joanna_wyn@bupt.edu.cn).

Hangyu Zhao is with the Chinese University of Hong Kong, Hong Kong SAR, China (e-mail: zhaohangyu@link.cuhk.edu.hk).

Xiaodong Xu and Ping Zhang are with the State Key Laboratory of Networking and Switching Technology, Beijing University of Posts and Telecommunications, Beijing 100876, China, and also with the Department of Broad-band Communication, Peng Cheng Laboratory, Shenzhen 518066, Guangdong, China (e-mail: xuxiaodong@bupt.edu.cn; pzhang@bupt.edu.cn).

Suyu Lv is with the School of Information Science and Technology, Beijing University of Technology, 100124, China (e-mail: lvsuyu@bjut.edu.cn).

Xiaofeng Tao is with the National Engineering Laboratory for Mobile Network Technologies, Beijing University of Posts and Telecommunications, 100876, China (e-mail: taoxf@bupt.edu.cn).

tection threshold is established to identify whether the signal is legal or not [11]. Since it is challenging to distinguish multi-users by establishing multi-thresholds, researchers have recently formulated the CSI-based multiuser PLA problem as a multi-classification problem and solved it via Machine Learning (ML) techniques [12], especially Deep Learning (DL) models [4], [13]–[15]. Liao et al. [13] introduce a DL-based PLA scheme to distinguish multiple legal users from attackers for mobile edge computing (MEC) systems, and adopt three gradient descent algorithms to reduce computation overheads. To avoid the overfitting issues of DL-based PLA models in MEC scenarios, Liao et al. [14] further present three data augmentation methods which can expand the richness of data sets by generating additional CSI samples. Additionally, Meng et al. [4] design two Latent Perturbed Neural Network (LPNN)-based PLA schemes, where Gaussian noises are added to the smooth latent layer to enhance the generalization capability of DL models in IIoT. Chen et al. [15] and Jing et al. [16] both combine Convolutional Neural Network (CNN), transfer learning, and data augmentation algorithms to speed up the training of PLA models for IoT scenarios.

Although various PLA approaches have been designed to enhance the authentication performance, the existing CSI-based PLA schemes still face the following challenges in authenticating multiple mobile industrial device.

- The first challenge involves enhancing the reliability of CSI fingerprints in low Signal-Noise-Ratio (SNR) environments. As crucial identity signatures, CSI fingerprints should be reliable and distinguishable. However, in low SNR areas, obtaining highly accurate CSI fingerprints becomes challenging due to severe multipath effects, interference from obstacles, and complex electromagnetic environments [17]. While approaches such as the multireceiver-based distributed framework proposed by [6] and [18] aim to mitigate fingerprint fluctuation caused by estimation errors and environmental noises, they may incur increases deployment costs and introduce new security risks.
- The second challenge lies in learning the inherent characteristics of users while considering the distribution deviation between training and testing CSI fingerprints resulting from users' movements. Meng et al. [4] utilize open-source industrial datasets to demonstrate that, the authentication accuracy of CSI-based schemes decreases as transmitters move away. This is due to the fact that CSI is a location-specific physical-layer attribute, and user movement leads to changes in the distribution of CSI. However, most existing schemes (e.g., [4], [6], [13]–[15]) assume that users are stationary and that the CSI fingerprint of each transmitter follows an independent and identically distributed pattern. Although Han et al. [19] compare the performance of their model-driven scheme with data-driven schemes using China Telecom's 5G channel model, they do not account for potential attacks. As a result, existing CSI-based physical-layer authentication schemes face challenges in accurately identifying mobile users under the threat of attacks.

To tackle the first challenge, we introduce Intelligent Reflecting Surfaces (IRSs) to strength the accuracy of CSI fingerprints. IRSs consist of numerous programmable units capable of manipulating and reflecting incoming signals. These programmable units allow IRSs to adjust the phase, amplitude, and direction of signals for control and optimization purposes [20]. By interacting with devices, IRSs can modify the signal propagation environment, thereby boosting signal strength and quality, improving communication capacity, and expanding coverage. For example, Cheng et al. [21] combine IRSs and Device-to-Device (D2D) communications to enable ultra-reliable and low-latency communication (URLLC) in IIoT. Therefore, leveraging IRSs enables us to mitigate multipath effects, reduce path loss, address signal blind spots, and ultimately enhance the reliability of CSI fingerprints.

To address the second challenge, we analyze CSI fingerprints of mobile users as time series data and employ graph convolutional networks (GCNs) to grasp the evolving patterns of fingerprints across time and space. Since the similarity of fingerprints decreases with users' distance, we model the fingerprints of mobile users as time series data to depict the dynamic changes of fingerprints during user movement. These sequences of fingerprint samples are then represented as graphs, where nodes denote each fingerprint sequence and edges signify the connections or interactions among them. GCNs excel at learning the topological structure and connections between nodes, making them ideal for handling intricate nonlinear relationships and assimilating local and global information among nodes. Consequently, GCNs can effectively capture both the spatio-temporal dynamics within individual time series and the interactions between them, thereby facilitating the authentication of mobile users' identities. The main contributions are summarized as follows.

- 1) To achieve reliable mobile multiuser authentication in EI-enabled IIoT, we propose the Temporal Dynamic Graph Convolutional Network (TDGCN)-based PLA scheme. IRSs enhance the distinguishability of CSI fingerprints through hierarchical channel estimation, while GNNs capture spatio-temporal dynamics.
- 2) CSI fingerprints are modeled as time series data, with dynamic GNNs capturing associations between them. Unlike CNNs, GNNs consider latent strong dependencies between each CSI dimension introduced by IRSs. Within each dynamic GNN, nodes and edges respectively represent CSI sequences and their interactions, with connections further represented by learnable adjacency matrices.
- 3) Temporal Convolutional Networks (TCNs) capture temporal dependencies within each CSI dimension. The length of learned features is synchronized with that of CSI sequences through padding operations before input into dynamic GNNs.
- 4) Dynamic Graph Isomorphism Networks (GINs) determine whether two graphs are structurally identical or isomorphic, aggregating information in parallel. Cascade node clustering pooling preserves learned information and reduces computational complexity.
- 5) Simulations on synthetic data demonstrate the superior

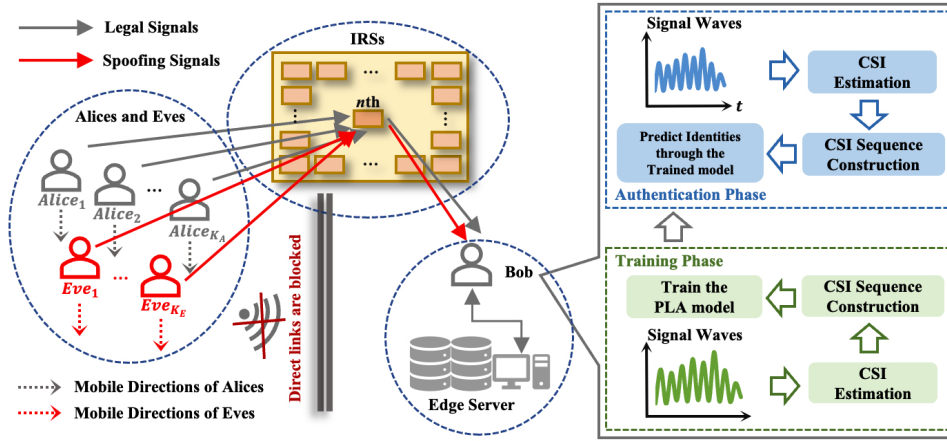


Fig. 1. Proposed mobile multiuser PLA model consisting of K_A legitimate industrial terminals ($Alice_1, Alice_2, \dots, Alice_{K_A}$), K_E spoofing attackers ($Eve_1, Eve_2, \dots, Eve_{K_E}$), and the legitimate receiver (Bob), based on the collected CSI fingerprints, the accuracy of which is enhanced by IRSs.

authentication accuracy of the proposed TDGCN-based PLA over seven typical ML-based PLA schemes.

II. SYSTEM MODEL AND PROBLEM FORMULATION

A. Network Model

As illustrated in Fig. 1, we consider a typical Alice-Eve-Bob model, and the nodes involved are described as follows.

Alices: K_A legal industrial terminals are in communication with the legitimate receiver (Bob) during different time slots. Alices are continuously moving to facilitate data collection or meet production line demands, thereby enhancing flexibility and enabling real-time analysis. The distance between transmitters is assumed to be greater than half a wavelength to ensure the distinguishability of their fingerprints [6], [8].

Eves: K_E spoofing attackers attempt to impersonate the identity information of the Alices, such as medium access control (MAC) addresses, to establish communication with Bob [5], [11]. Eves are dynamically altering illicit fingerprints while in motion, aiming to befuddle Bob.

IRSs: Owing to electromagnetic interference from equipment, signal dead zones or attenuation resulting from building structures and obstacles, and signal fluctuations resulting from the activities of workers and robots, the channel fingerprints of terminals are difficult to distinguish [6]. Considering that IRSs can enhance signal propagation through diversified paths, stabilizes signal quality, reduces distortion and interference, and dynamically adjusts to optimize signal transmission [20], we introduce IRSs to enhance the accuracy and reliability of channel fingerprints. The direct links between Alices/Eves and Bob are assumed to be blocked [22].

Bob: Bob is positioned at the edge of IIoT to conveniently collect fingerprint samples of terminals, and is equipped with edge servers that offer ample computing power to train the authentication model [7], [12], [13]. Bob's responsibility is to identify the transmitter of the received signal using the trained authenticator.

B. Channel Model

The received signal at Bob is represented as

$$\mathbf{b}_s = \mathbf{x}\mathbf{a}_s + \mathbf{n}, \quad (1)$$

where \mathbf{a}_s denotes the signal transmitted from Alices/Eves and $\mathbf{n} \sim \mathcal{CN}(0, \sigma^2)$ represents the Gaussian noises. $\mathbf{x} = \mathbf{h}\boldsymbol{\psi}\mathbf{g}$ denotes the cascade channel matrix from Alices/Eves to Bob through IRSs, where $\boldsymbol{\psi}$ represents the element response matrix of IRSs, \mathbf{g} and \mathbf{h} respectively denote the channel matrices from Alices/Eves to IRSs and from IRSs to Bob. Hierarchical CSI fingerprints \mathbf{x} can be acquired through channel estimation, which is not the primary focus of this paper and have been realized by various methods, including tensor decomposition, compressive sensing, and DL models [23].

C. Problem Formulation

We consider a multiple-input multiple-output (MIMO) scene, and let N_T and N_R respectively denote the number of antennas of Alices/Eves and Bob. The hierarchical CSI fingerprints are multidimensional matrices associated with the positions of devices. Therefore, in moving scenarios, CSI fingerprints can be modeled as multivariate time series (MTS) $\mathbf{X} = \{\mathbf{x}_1, \mathbf{x}_2, \dots, \mathbf{x}_d\} \in \mathbb{R}^{d \times l}$, where $d = 2N_R N_T$ denotes the dimension of CSI fingerprints and $l \in \mathbb{N}^*$ represents the length of CSI fingerprint series. $\mathbf{x}_i = \{x_{i,1}, x_{i,2}, \dots, x_{i,l}\}$ ($i \in [1, d]$) represents the sequence of the i -th dimension feature in the multi-dimensional CSI fingerprint. The mobile multiuser PLA problem involves formulating a classifier $f(\cdot)$ from $\chi = \{\mathbf{X}_1, \mathbf{X}_2, \dots, \mathbf{X}_M\}$ to $\eta = \{\mathbf{y}_1, \mathbf{y}_2, \dots, \mathbf{y}_M\}$ to predict the identity label \mathbf{y}_m corresponding to the CSI fingerprint sequence \mathbf{X}_m ($m = [1, M]$).

III. TDGCN-BASED MOBILE MULTIUSER PLA

As depicted in Fig. 2, the proposed TDGCN-based PLA scheme comprises several key modules. Initially, the CSI pre-processing module segments the estimated CSI fingerprints \mathbf{x} into temporal sequences \mathbf{X} , while the graph initialization module generates adjacency matrices \mathbf{A} for each CSI

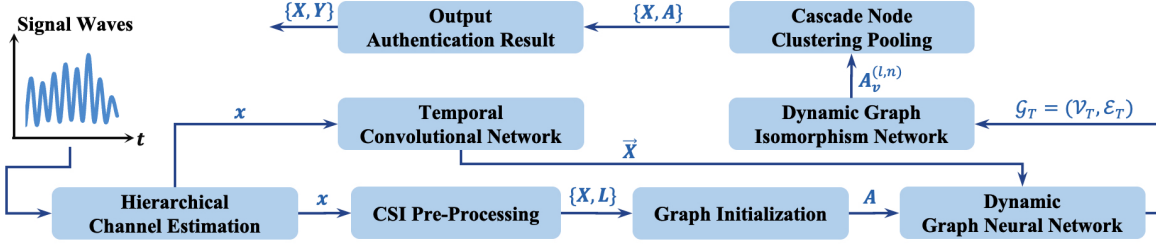


Fig. 2. Proposed TDGCN-based PLA scheme.

sequence. Subsequently, the TCN module uncovers temporal dependencies within each dimension of the CSI fingerprint x . The GNN module captures dynamic associations between CSI sequences \mathbf{X} , with the dynamic GIN module aggregating this information. To reduce computational complexity and enhance generalization ability, the cascade node clustering pooling module is employed. Finally, the authentication result output module retrieves the identities of input CSI sequences.

A. CSI Pre-Processing Module

The training dataset $\mathcal{D}_{\text{train}}$ and testing dataset $\mathcal{D}_{\text{test}}$ are used to train the mobile multiuser authentication model and verify its authentication performance. $\mathcal{D}_{\text{train}}$ is composed of CSI fingerprint sequences $\mathbf{X}_{\text{train}}$ and corresponding labels $\mathbf{Y}_{\text{train}}$, which are respectively denoted by

$$\mathbf{X}_{\text{train}} = \underbrace{[\mathbf{X}_1^1, \dots, \mathbf{X}_1^{N_1}]}_{N_1}, \underbrace{[\mathbf{X}_2^1, \dots, \mathbf{X}_2^{N_2}]}_{N_2}, \dots, \underbrace{[\mathbf{X}_K^1, \dots, \mathbf{X}_K^{N_K}]}_{N_K} \quad (2)$$

and

$$\mathbf{Y}_{\text{train}} = \underbrace{[\mathbf{L}_1, \dots, \mathbf{L}_1]}_{N_1}, \underbrace{[\mathbf{L}_2, \dots, \mathbf{L}_2]}_{N_2}, \dots, \underbrace{[\mathbf{L}_K, \dots, \mathbf{L}_K]}_{N_K}, \quad (3)$$

where N_k is the number of CSI fingerprint sequences of the k -th ($k \in [1, K]$) transmitter and $K = K_A + K_E$ is the number of transmitters. \mathbf{L}_k is the identity label of the k -th transmitter, represented by one-hot coding as $\mathbf{L}_k = [0, \dots, 1, \dots, 0]^T$, where the k -th element is 1 and the others are 0. The CSI sequences of each transmitter are evenly divided by some equidistant time slots $T = \{T_1, T_2, \dots, T_N\}$ arranged in time sequence, where $N = N_1 = \dots = N_K$ is the number of time slots.

B. Graph Initialization Module

Remark 1. CNNs have been extensively employed to capture the spatial-frequency features of multidimensional CSI fingerprints in MIMO systems, as seen in [4], [9], [13]. However, existing CNN-based PLA models often overlook the latent dependency relationships between each CSI dimension. With the introduction of IRSs, wireless environments between transmitters and Bob undergo changes, resulting in strong correlations between various dimensional features of CSI fingerprints. Recognizing that the above dependency relationships can be naturally represented as graphs, we propose a graph-based approach to address this challenge.

The fundamental structure of a graph consists of nodes and edges, commonly denoted as $\mathcal{G} = (\mathcal{V}, \mathcal{E})$. Nodes \mathcal{V}

represent CSI fingerprint sequences and are the basic building blocks of the graph \mathcal{G} . Edges \mathcal{E} serve as connectors between nodes \mathcal{V} , revealing the relationships and interactions among them. Edges \mathcal{E} can be either directed or undirected, and they can be assigned weights to quantify the strength or significance of connections between nodes \mathcal{V} . Compared with traditional graph structures, GNNs can produce more enriched and insightful node representations leveraging DL-based node learning and updating continually.

The latent relationships between CSI sequences \mathbf{X} are modeled by the adjacency matrix. Firstly, the similarity matrix \mathbf{S} between each dimension fingerprint x is calculated by

$$S_{ij} = \frac{\exp(-\sigma_{\text{ReLU}}(d_{\text{Eu}}(x_i, x_j)))}{\sum_{m=1}^d \exp(-\sigma_{\text{ReLU}}(d_{\text{Eu}}(x_i, x_m)))}, \quad (4)$$

where $\sigma_{\text{ReLU}}(x) = \max(0, x)$ denotes the Rectified Linear Unit (ReLU) activation function and $d_{\text{Eu}}(x_i, x_j)$ represents the Euclidean distance between x_i and x_j . Then, the adjacency matrix \mathbf{A} is obtained by $\mathbf{A} = \sigma_{\text{ReLU}}(\mathbf{S}\mathbf{\Upsilon})$, where $\mathbf{\Upsilon}$ represents learnable parameters. Moreover, \mathbf{A} undergoes a sparsification process, wherein a significant portion of its elements is set to 0, rendering the matrix sparser and reducing the computational load. Specifically, the threshold θ is introduced for normalization as $A_{ij} = \begin{cases} A_{ij}, & A_{ij} \geq \theta \\ 0, & A_{ij} < \theta \end{cases}$

C. Temporal Convolutional Network Module

The Temporal Convolutional Network (TCN) module is designed to capture the temporal dependencies between $x_{i,1}$, $x_{i,2}$, ..., and $x_{i,l}$. It integrates multiple convolution layers with distinct kernels to grasp local characteristics. The extracted features in the l -th CNN layer are represented as

$$\mathbf{Z}_l = \sigma_{\text{ReLU}}(\mathbf{W}_l * \mathbf{Z}_{l-1} + \mathbf{B}_l), \quad (5)$$

where \mathbf{Z}_{l-1} is both the output of the $(l-1)$ -th CNN layer and the input of the l -th CNN layer, $*$ is the convolution operation, and \mathbf{W}_l and \mathbf{B}_l are the weight and bias matrices in the l -th CNN layer, respectively. Causal convolution is employed to guarantee the forward propagation of information during convolution operations [24]. Padding operations are subsequently employed to synchronize the length of the output features $\bar{\mathbf{X}}$ with that of CSI fingerprint sequences \mathbf{X} .

D. Dynamic Graph Neural Network Module

Remark 2. GNNs are categorized into static and dynamic graphs. Static graphs are ideal for unchanged topological

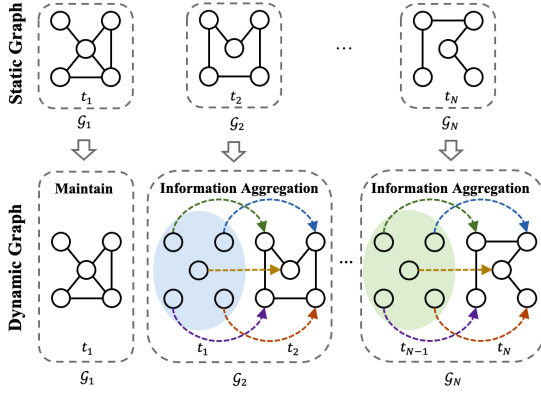


Fig. 3. Dynamic Graph Transformation.

structures, such as user relationship graphs in social networks, while dynamic graphs excel at managing evolving graph structures and attributes, like traffic networks where vehicle positions change over time. In mobile scenarios, shifts in user positions lead to continual changes in CSI fingerprint distribution. Consequently, dynamic graphs are utilized to capture the temporal dynamics of CSI fingerprint sequences.

For a set of fixed nodes \mathcal{V} , the dynamic graph is usually represented as

$$\mathcal{G}_T = (\mathcal{V}, \mathcal{E}_T), \quad (6)$$

where $\mathcal{G}_T = \{\mathcal{G}_{T_1}, \dots, \mathcal{G}_{T_N}\}$ and $\mathcal{E}_T = \{\mathcal{E}_{T_1}, \dots, \mathcal{E}_{T_N}\}$. However, as transmitters move, the nodes \mathcal{V} representing fingerprint sequences \mathbf{X} are no longer fixed, but vary with channel environments. Therefore, (6) is inappropriate, and we instead introduce the dynamic graph as

$$\mathcal{G}_T = (\mathcal{V}_T, \mathcal{E}_T). \quad (7)$$

We assume that the CSI fingerprint sequence evolve from its earlier time slots through information aggregation. As depicted in Fig. 3, except for the graph \mathcal{G}_{T_1} corresponding to the first fingerprint sequence \mathbf{X}^1 , l nodes are introduced to each subsequent graph \mathcal{G}_n to represent the node characteristics \mathcal{V}^{n-1} in the graph \mathcal{G}_{n-1} corresponding to the preceding fingerprint sequence \mathbf{X}^{n-1} . Directed edges are then established between the nodes \mathcal{V}^{n-1} of the previous fingerprint sequence \mathbf{X}^{n-1} and the nodes \mathcal{V}^{n-1} of the current fingerprint sequence \mathbf{X}^n to represent associations. These new directed edges aggregate the nodes \mathcal{V}^{n-1} from the previous graph \mathcal{G}_{n-1} into the nodes \mathcal{V}^n of the current graph \mathcal{G}_n , after which the source nodes \mathcal{V}^{n-1} are removed to maintain consistent node counts across all graphs $\{\mathcal{G}_2, \dots, \mathcal{G}_N\}$ relative to the first graph \mathcal{G}_1 .

E. Dynamic Graph Isomorphism Network Module

GINs are hailed as leading variants of GNNs, boasting discriminative and representational prowess comparable to the Weisfeiler-Lehman (WL) graph isomorphism test [25]. GINs update node representations as

$$\mathbf{A}_v^{l+1} = \text{MLP}^l \left((1 + \epsilon^l) \mathbf{A}_v^l + \sum_{u \in \mathcal{N}(v)} \mathbf{A}_u^l \right), \quad (8)$$

where \mathbf{A}_v^l is the adjacency matrix of the v -th node in the l -th layer, ϵ^l denotes learnable parameters, and MLP represents Multilayer Perceptron. In contrast to traditional GNNs, GINs replace the mean aggregator with a sum aggregator for nodes and ensure each neighbor contributes equally to updating the central node. Additionally, GINs amalgamate information from all layers of nodes to derive the final representation as

$$\mathbf{A} = \text{CONCAT} \left(\sum_{k=0}^L \mathbf{A}_v^k \right), \quad (9)$$

where CONCAT is the concatenate function.

Remark 3. Due to different time slot CSI sequences in mobile scenes, (8) and (9) are not suitable for dynamic GNNs. Motivated by [26], Dynamic GINs are employed to aggregate information from different sets of nodes as

$$\mathbf{A}_v^{(l,n)} = \text{MLP}^{(l,n)} \left((1 + \epsilon^l) \cdot \mathbf{A}_v^{(l-1,n)} + \mathbf{A}_v^{(l-1,n-1)} + \sum_{u \in \mathcal{N}(v)} \tilde{\omega}_{ij} \cdot \mathbf{A}_u^{(l-1,n)} \right) \quad (10)$$

and

$$\mathbf{A}_v^l = \text{CONCAT} \left(\sum_{n=1}^N \mathbf{A}_v^{(l,n)} \right), \quad (11)$$

where $\mathbf{A}_v^{(l,n)}$ denotes the adjacency matrix for the v -th node at the n -th time slot in the l -th layer, and $\tilde{\omega}_{ij}$ represents the normalized weights of edges.

F. Cascade Node Clustering Pooling Module

Graph pooling is a pivotal component of GNNs, which is similar to the role of pooling operations in traditional neural networks. Its purpose is to diminish the graph's scale, decrease computational complexity, and distill crucial graph features. By aggregating nodes or subgraphs into higher-level representations, graph pooling operations enhance the model's comprehension of the graph's structure and content, thereby boosting its generalization ability [27].

As illustrated in Fig. 4, the cascade node clustering pooling module views graph pooling as a node clustering problem, where nodes are mapped into clusters, forming new nodes for the coarsened graph. The cluster assignment matrices predict node assignments in the l -th layer as

$$\mathbf{C}^l = f_{\text{CA}}(\mathbf{X}^l, \mathbf{A}^l), \quad (12)$$

where f_{CA} denotes the cluster assignment function. Subsequently, new graphs with fewer nodes then are obtained as

$$\{\mathbf{X}^{l+1}, \mathbf{A}^{l+1}\} = f_{\text{GC}}(\mathbf{X}^l, \mathbf{A}^l, \mathbf{C}^l), \quad (13)$$

where f_{GC} symbolizes the graph coarsening function.

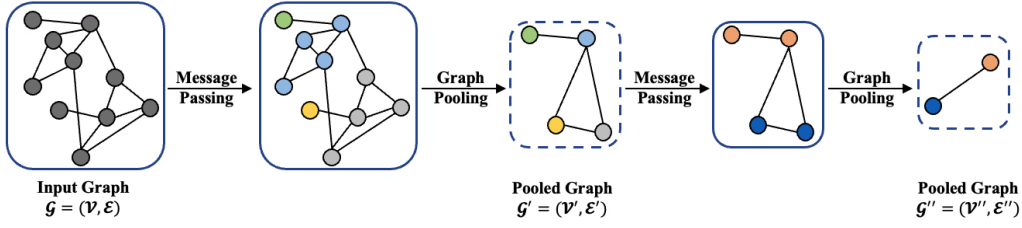


Fig. 4. Cascade node clustering pooling.

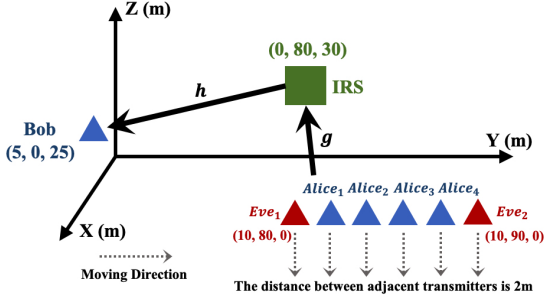


Fig. 5. Positions of Alices, Eves, IRSs and Bob, where the positions of Alices are (10, 82/84/86/88, 0)

G. Authentication Result Output Module

The module employs average pooling to compute the average of graph features, yielding a fixed-length vector. Subsequently, this vector is mapped to a logical vector via a fully connected layer, culminating in the authentication result being derived through the softmax function. The loss function is given as $\mathcal{L} = -\frac{1}{N} \sum_{i=1}^{N \cdot K} \sum_{j=1}^K \mathbf{y}_{ij} \log \hat{\mathbf{y}}_{ij}$, where \mathbf{y}_{ij} and $\hat{\mathbf{y}}_{ij}$ are real and predicted identity labels, respectively.

IV. SIMULATION RESULTS AND ANALYSIS

A. Performance Metric

False alarm rate and miss detection rate are typically used to gauge the reliability of PLA models. However, these coarse-grained metrics might not be suitable for multiuser scenarios as they overlook which legal or illegal transmitter the received signal originates from. Thus, drawing inspiration from [4], [6], [14], [16], the reliability of the proposed multiuser PLA model is evaluated by the fine-grained authentication metric: authentication accuracy, defined as

$$P_{\text{accuracy}} = \frac{1}{N \cdot K} \sum_{n=1}^{N \cdot K} \mathbb{I}(\mathbf{L}_n = \mathbf{Y}_n), \quad (14)$$

where $N \cdot K$ is the number of CSI fingerprint sequences, \mathbf{L}_n and \mathbf{Y}_n represent actual and predicted identity labels of the n -th CSI fingerprint sequences, respectively. \mathbb{I} is the indicator function, defined as $\mathbb{I}(\cdot) = \begin{cases} 1, & \cdot \text{ is true} \\ 0, & \cdot \text{ is false} \end{cases}$.

B. Simulation Parameters

As illustrated in Fig. 5, four legal transmitters and two spoofing attackers are considered. CSI fingerprints are gener-

TABLE I
SIMULATION AND HYPER PARAMETERS

Parameters	Values
Number of antennas of each transmitter N_T	4
Number of antennas of Bob N_R	3
Number of IRS elements	8*16
Carrier Frequency	3.5 GHz
Rice factors κ_h and κ_g	3 and 4
Bandwidth	1 MHz
Speed of Transmitters	2 m/s
CSI sampling frequency	100 Hz
Number of each transmitter's CSI samples	50000
Number of each transmitter's CSI sequences	1000
Length of each CSI sequence	50
Number of each transmitter's training CSI samples	30000
Number of each transmitter's testing CSI samples	20000
Learning rate	0.0001
Batch size	16
The number of GNN layers	3
Time convolutional kernel size for each layer	9, 5, and 3
The ratio of pooling for nodes	0.2
Decrease rate of weights	0.0001
Seed for initializing training	42

ated through MatLab. \mathbf{h} and \mathbf{g} are modeled as Rician Channel as

$$\mathbf{h} = \sqrt{\frac{PL_h^{LoS} \kappa_h}{1 + \kappa_h}} \bar{\mathbf{h}} + \sqrt{\frac{PL_h^{NLoS}}{1 + \kappa_h}} \tilde{\mathbf{h}} \quad (15)$$

$$\mathbf{g} = \sqrt{\frac{PL_g^{LoS} \kappa_g}{1 + \kappa_g}} \bar{\mathbf{g}} + \sqrt{\frac{PL_g^{NLoS}}{1 + \kappa_g}} \tilde{\mathbf{g}} \quad (16)$$

where $\bar{\mathbf{h}}$ and $\bar{\mathbf{g}}$ are LoS paths, and $\tilde{\mathbf{h}}$ and $\tilde{\mathbf{g}}$ are NLoS paths. The path loss PL is modeled according to 3GPP TR 38.901. The LoS paths are modeled according to [28], while the NLoS paths are modeled as Rayleigh fading models. The simulation parameters are given in Tab. I in detail. The computer configurations are Intel Core i5-13600KF, 3.50 GHz basic frequency, and 32 GB of RAM.

C. Baseline Models

The proposed method is compared with seven PLA models, including Decision Tree (DT) [12], K -Nearest Neighbor (KNN) [12], Naive Bayesian (NB) [29], Weighted Voting (WV) [7], Gradient Boosting Decision Tree (GBDT) [30], Regularized Gradient Boosting Optimization (RGBO) [6], and Improved Gradient Boosting Optimization (IGBO) [6].

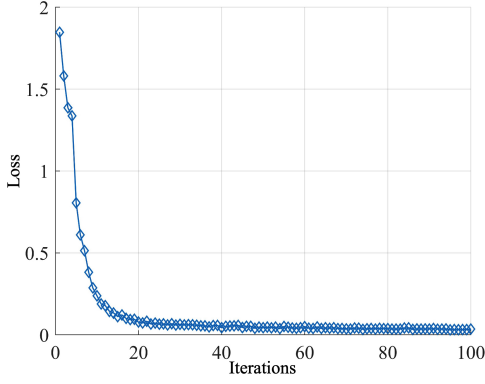


Fig. 6. Loss function versus different iteration numbers.

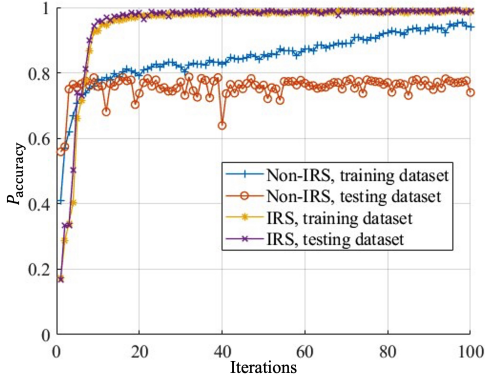


Fig. 7. Authentication accuracy versus different iteration numbers with or without IRS assistance.

D. Simulation Results

Convergence performance. As illustrated in Fig. 6, the training loss is depicted against iteration numbers. By the 30th iteration, the model demonstrates near convergence, while by the 40th iteration, complete convergence is achieved. The rapid convergence of the proposed scheme is validated by Fig. 6.

Effectiveness of IRSs. Fig. 7 depicts the authentication accuracy in relation to iteration numbers, comparing scenarios with and without IRSs. In the absence of IRSs, the directed channels between Alices/Eves and Bob are modeled as Rayleigh channels due to significant attenuation. With IRSs present, both the training and testing datasets exhibit swift convergence. Conversely, in their absence, the training dataset shows slower convergence, while the testing dataset's performance fluctuates. Notably, with IRSs, both training and testing dataset's authentication accuracy approaches 100%. Conversely, without IRSs, the testing dataset's authentication accuracy falls below 80%. Fig. 7 validates that the presence of IRSs can enhance authentication accuracy by at least 25%.

Performance under different SNRs. Fig. 8 and Fig. 9 showcase the authentication accuracy across varying SNRs, with artificial noise added to simulate noisy environments. Under ideal CSI conditions, the proposed scheme achieves 100% authentication accuracy. As SNRs decrease, authentication accuracy remains nearly 100% in the training dataset but gradually deteriorates in the testing dataset. Conversely, as SNRs increase, baseline schemes show gradual improve-

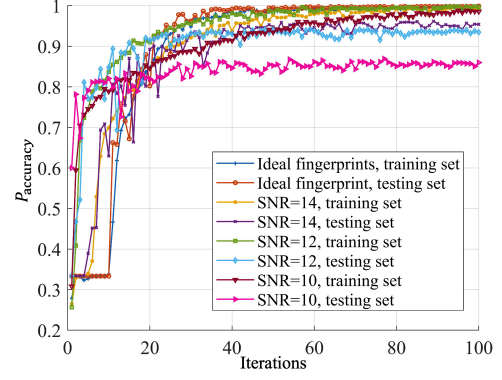


Fig. 8. Authentication accuracy of the proposed TDGCN-based PLA scheme versus different iteration numbers under different SNRs.

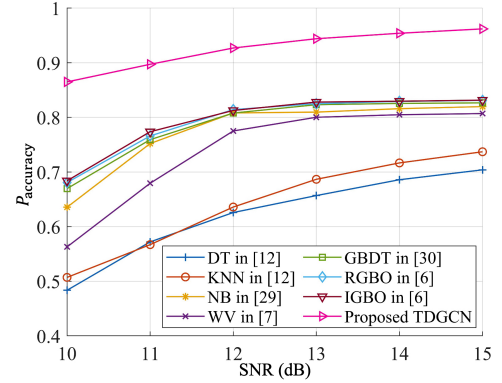


Fig. 9. Authentication accuracy of different PLA schemes versus SNRs.

ment in authentication accuracy. However, regardless of SNR levels, the proposed scheme consistently outperforms baseline methods due to its consideration of CSI fingerprint distribution changes caused by user movements, whereas other methods assume independent and identical distribution of CSI fingerprints for each user. At the SNR of 15 dB, the proposed scheme demonstrates an improvement in authentication accuracy ranging from 13.04% to 36.64%.

Performance versus user distances. Fig. 10 contrasts the authentication accuracy of various PLA schemes against transmitter distances. As the distance between users decreases,

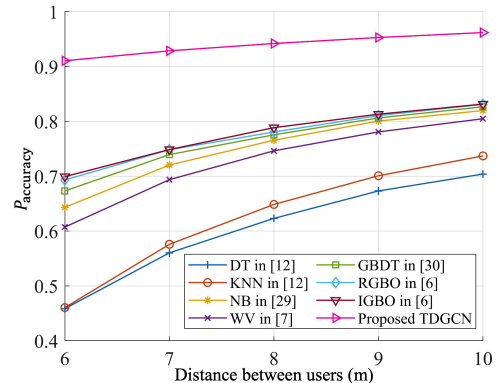


Fig. 10. Authentication accuracy of different PLA schemes versus different distances between users.

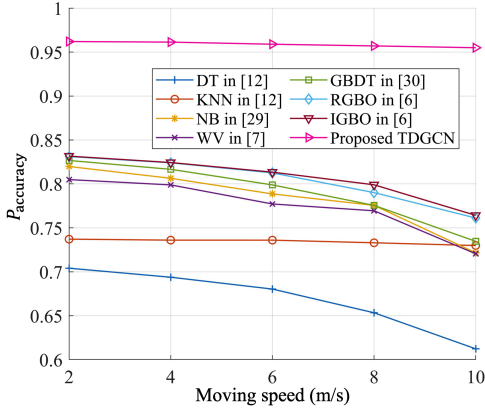


Fig. 11. Authentication accuracy of different PLA schemes versus different moving speeds of users.

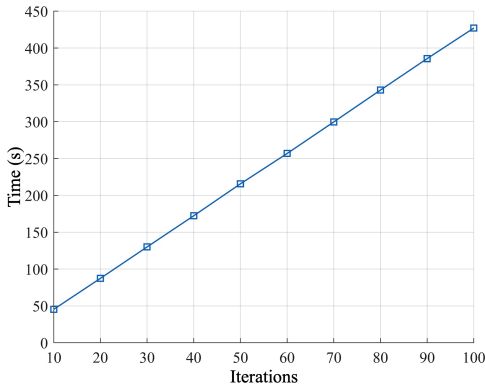


Fig. 12. Authentication time versus different iteration numbers.

the similarity of fingerprints increases, resulting in higher distribution coincidence, thus making it more challenging for the authentication model to differentiate, consequently lowering authentication accuracy. Nevertheless, the proposed scheme consistently outperforms baseline methods by capturing dynamic temporal-spatio features. Fig. 10 further validates the superiority of the proposed approach.

Performance versus user speeds. Fig. 11 analyzes the authentication accuracy of different schemes versus user speeds. As users move faster, the distance between adjacent fingerprints increases under the same CSI sampling frequency, leading to lower distribution similarity and decreased performance for most distribution-based authentication models. Although KNN relies on CSI sample distances and is less affected, its feature learning capability is limited, resulting in significantly lower authentication accuracy compared to the proposed TDGCN-based scheme.

Training complexity. Fig. 12 shows the training time versus iteration numbers, and it increases almost linearly.

V. CONCLUSIONS

This paper introduces a TDGCN-based PLA scheme, aimed at identifying mobile multi-users in EI-aided IIoT. IRSs are strategically placed to augment the accuracy of CSI fingerprints. Leveraging TCNs and dynamic GNNs, the model learns the temporal evolution of each CSI dimension feature and the

spatio-temporal dynamics between CSI sequences. Dynamic GINs and cascade pooling mechanisms are utilized to retain learned information while mitigating computational complexity. Simulation results confirm the efficacy of the proposed scheme. Additionally, future work will explore the integration of reinforcement learning to optimize IRS parameters.

REFERENCES

- [1] R. Tallat, A. Hawbani, X. Wang, A. Al-Dubai, L. Zhao, Z. Liu, G. Min, A. Y. Zomaya, and S. Hamood Alsamhi, "Navigating industry 5.0: A survey of key enabling technologies, trends, challenges, and opportunities," *IEEE Commun. Surv. Tutor.*, vol. 26, no. 2, pp. 1080–1126, 2024.
- [2] H. Gu, L. Zhao, Z. Han, G. Zheng, and S. Song, "Ai-enhanced cloud-edge-terminal collaborative network: Survey, applications, and future directions," *IEEE Commun. Surv. Tutor.*, vol. 26, no. 2, pp. 1322–1385, 2024.
- [3] B. Mao, J. Liu, Y. Wu, and N. Kato, "Security and privacy on 6g network edge: A survey," *IEEE Commun. Surv. Tutor.*, vol. 25, no. 2, pp. 1095–1127, 2023.
- [4] R. Meng, X. Xu, H. Sun, H. Zhao, B. Wang, S. Han, and P. Zhang, "Multiuser physical-layer authentication based on latent perturbed neural networks for industrial internet of things," *IEEE Internet of Things J.*, vol. 10, no. 1, pp. 637–652, 2023.
- [5] H. Fang, Z. Xiao, X. Wang, L. Xu, and L. Hanzo, "Collaborative authentication for 6g networks: An edge intelligence based autonomous approach," *IEEE Trans. Inf. Forensics Secur.*, vol. 18, pp. 2091–2103, 2023.
- [6] R. Meng, X. Xu, H. Zhao, B. Wang, G. Li, B. Xu, and P. Zhang, "Multiobservation-multichannel-attribute-based multiuser authentication for industrial wireless edge networks," *IEEE Trans. Ind. Informat.*, vol. 20, no. 2, pp. 2097–2108, 2024.
- [7] F. Xie, Z. Pang, H. Wen, W. Lei, and X. Xu, "Weighted voting in physical layer authentication for industrial wireless edge networks," *IEEE Trans. Ind. Informat.*, vol. 18, no. 4, pp. 2796–2806, 2021.
- [8] N. Xie, Z. Li, and H. Tan, "A survey of physical-layer authentication in wireless communications," *IEEE Commun. Surv. Tutor.*, vol. 23, no. 1, pp. 282–310, 2020.
- [9] N. Gao, Q. Huang, C. Li, S. Jin, and M. Matthaiou, "Esanet: Environment semantics enabled physical layer authentication," *IEEE Wirel. Commun. Lett.*, vol. 13, no. 1, pp. 178–182, 2024.
- [10] G. Oliveri, S. Sciancalepore, S. Raponi, and R. Di Pietro, "Past-ai: Physical-layer authentication of satellite transmitters via deep learning," *IEEE Trans. Inf. Forensics Secur.*, vol. 18, pp. 274–289, 2022.
- [11] L. Xiao, L. J. Greenstein, N. B. Mandayam, and W. Trappe, "Using the physical layer for wireless authentication in time-variant channels," *IEEE Trans. Wirel. Commun.*, vol. 7, no. 7, pp. 2571–2579, 2008.
- [12] F. Pan, Z. Pang, H. Wen, M. Luvisotto, M. Xiao, R.-F. Liao, and J. Chen, "Threshold-free physical layer authentication based on machine learning for industrial wireless cps," *IEEE Trans. Ind. Informat.*, vol. 15, no. 12, pp. 6481–6491, 2019.
- [13] R.-F. Liao, H. Wen, J. Wu, F. Pan, A. Xu, H. Song, F. Xie, Y. Jiang, and M. Cao, "Security enhancement for mobile edge computing through physical layer authentication," *IEEE Access*, vol. 7, pp. 116 390–116 401, 2019.
- [14] R.-F. Liao, H. Wen, S. Chen, F. Xie, F. Pan, J. Tang, and H. Song, "Multiuser physical layer authentication in internet of things with data augmentation," *IEEE internet of things j.*, vol. 7, no. 3, pp. 2077–2088, 2019.
- [15] Y. Chen, P.-H. Ho, H. Wen, S. Y. Chang, and S. Real, "On physical-layer authentication via online transfer learning," *IEEE Internet Things J.*, vol. 9, no. 2, 2022.
- [16] T. Jing, H. Huang, Q. Gao, Y. Wu, Y. Huo, and Y. Wang, "Multi-user physical layer authentication based on csi using resnet in mobile iiot," *IEEE Trans. Inf. Forensics Secur.*, 2023.
- [17] V.-L. Nguyen, P.-C. Lin, B.-C. Cheng, R.-H. Hwang, and Y.-D. Lin, "Security and privacy for 6g: A survey on prospective technologies and challenges," *IEEE Commun. Surv. Tutor.*, vol. 23, no. 4, pp. 2384–2428, 2021.
- [18] T. Zhang, Y. Huo, Q. Gao, L. Ma, Y. Wu, and R. Li, "Cooperative physical layer authentication with reputation-inspired collaborator selection," *IEEE Internet of Things J.*, 2023.

- [19] J. Han, Y. Li, G. Liu, J. Ma, Y. Zhou, H. Fang, and X. Wu, "Model-driven learning for physical layer authentication in dynamic environments," *IEEE Commun. Lett.*, 2024.
- [20] C. Pan, G. Zhou, K. Zhi, S. Hong, T. Wu, Y. Pan, H. Ren, M. Di Renzo, A. L. Swindlehurst, R. Zhang *et al.*, "An overview of signal processing techniques for ris/firs-aided wireless systems," *IEEE J. Sel. Top. Signal Process.*, vol. 16, no. 5, pp. 883–917, 2022.
- [21] J. Cheng, C. Shen, Z. Chen, and N. Pappas, "Robust beamforming design for irls-aided urllc in d2d networks," *IEEE Trans. Commun.*, vol. 70, no. 9, pp. 6035–6049, 2022.
- [22] Y. Liu, X. Mu, X. Liu, M. Di Renzo, Z. Ding, and R. Schober, "Reconfigurable intelligent surface-aided multi-user networks: Interplay between noma and ris," *IEEE Wireless Communications*, vol. 29, no. 2, pp. 169–176, 2022.
- [23] B. Zheng, C. You, W. Mei, and R. Zhang, "A survey on channel estimation and practical passive beamforming design for intelligent reflecting surface aided wireless communications," *IEEE Commun. Surv. Tutor.*, vol. 24, no. 2, pp. 1035–1071, 2022.
- [24] H. Sun and T. Wang, "Toward causal-aware rl: State-wise action-refined temporal difference," 2022. [Online]. Available: <https://arxiv.org/abs/2201.00354>
- [25] H. Maron, H. Ben-Hamu, H. Serviansky, and Y. Lipman, "Provably Powerful Graph Networks," in *Advances in Neural Information Processing Systems*, vol. 32. Curran Associates, Inc., 2019.
- [26] H. Liu, X. Liu, D. Yang, Z. Liang, H. Wang, and C. Yong, "Todynet: Temporal dynamic graph neural network for multivariate time series classification," 2023. [Online]. Available: <https://arxiv.org/abs/2304.05078>
- [27] C. Liu, Y. Zhan, J. Wu, C. Li, B. Du, W. Hu, T. Liu, and D. Tao, "Graph pooling for graph neural networks: progress, challenges, and opportunities," in *Proceedings of the Thirty-Second International Joint Conference on Artificial Intelligence*, ser. IJCAI '23, 2023.
- [28] X. Hu, C. Masouros, and K.-K. Wong, "Reconfigurable intelligent surface aided mobile edge computing: From optimization-based to location-only learning-based solutions," *IEEE Trans. Commun.*, vol. 69, no. 6, pp. 3709–3725, 2021.
- [29] S. Denis, A. Kaya, R. Berkvens, and M. Weyn, "Device-free localization and identification using sub-ghz passive radio mapping," *Appl. Sci.*, vol. 10, no. 18, p. 6183, 2020.
- [30] M. Douiba, S. Benkirane, A. Guezzaz, and M. Azrour, "An improved anomaly detection model for IoT security using decision tree and gradient boosting," *J. Supercomput.*, vol. 79, no. 3, pp. 3392–3411, 2023.